Journal of Building Engineering 63 (2023) 105511

Contents lists available at ScienceDirect

Journal of Building Engineering

journal homepage: www.elsevier.com/locate/jobe

Shear strengthening of masonry walls with Textile Reinforced Mortars (TRM) under high temperature exposure

L. Estevan *, B. Torres, F.B. Varona, F.J. Baeza, S. Ivorra

Department of Civil Engineering, University of Alicante, P.O. Box 99, 03080, Alicante, Spain

ARTICLE INFO

Keywords:
Masonry
In-plane behavior
Shear strengthening
TRM
High temperature
Diagonal compression

ABSTRACT

The behavior of masonry walls strengthened with Textile Reinforced Mortars (TRM) is a topic that has received considerable attention from researchers in recent years. However, the response of such elements after exposure to high temperature is an issue that remains to be explored extensively. This study analyzes the behavior of TRM-strengthened brick masonry panels with glass and carbon fiber meshes subjected to temperatures up to 600 °C, and subsequently tested under diagonal compression. The reinforcements were applied before or after temperature exposure, to analyze the effectiveness of damaged or undamaged TRMs, thus simulating different scenarios that might occur in a real building under a fire event. In general terms, the results showed that TRMs with carbon fibers exhibited a better response in these conditions, restoring the walls to their original capacity and providing additional ductility, whilst reinforcements with glass fibers seemed to be more affected by temperature. Finally, the experimental results are here compared to predictions from available design guides, in order to assess the accuracy that these codes would provide in these circumstances.

1. Introduction

A large part of the buildings that make up our heritage are built with load-bearing walls, usually made of stone, masonry or brickwork. These structures are particularly vulnerable to extraordinary actions such as earthquakes, as has been observed in recent decades in various regions of Italy, for example [1,2]. In most cases, these buildings were built according to usual construction practices of the time but, in general, they do not meet the requirements of modern standards. For this reason, the safety of these structures is a major problem, most notably in the case of public, administrative, residential or religious buildings, for example.

In recent years, the scientific community has focused on Textile Reinforced Mortars (TRM), also known as Fiber Reinforced Cementitious Matrix (FRCM), to provide a potential reinforcement solution for this type of constructions [3]. Basically, these systems consist of the incorporation of one or several meshes of glass, carbon, or basalt fibers (among other materials) embedded in a mortar matrix, obtaining a very thin layer of material (usually in the order of 10–15 mm) that hardly consumes any space. In the context of stone or masonry constructions, TRMs have significant advantages over Fiber Reinforced Polymers (FRP), due to their better compatibility with the substrates to be reinforced, their permeability to water vapor, their reversibility and their better fire performance, for example [4,5]. TRMs have demonstrated their effectiveness in a number of scenarios such as wall reinforcement [6–8], column confinement [9,10] or intervention in elements such as arches or vaults [11,12], just to name but a few successful applications.

On the other hand, one of the main aspects governing the response of masonry structural elements to horizontal actions is the shear

* Corresponding author.
E-mail address: luis.estevan@ua.es (L. Estevan).

https://doi.org/10.1016/j.jobe.2022.105511
Received 27 June 2022; Received in revised form 13 October 2022; Accepted 2 November 2022
Available online 5 November 2022
2352-7102/© 2022 The Authors. Published by Elsevier Ltd. This is an open access article under the CC BY-NC-ND license (http://creativecommons.org/licenses/by-nc-nd/4.0/).

resistance of the walls to in-plane forces [13,14]. Much research has been carried out in recent years to analyze the effect of TRM strengthening in these conditions, and several valuable studies have been reported in the literature. These have been carried out on both stone or masonry [15–22] and brick walls [18,23–31], which had undergone diagonal compression testing, usually in accordance with the procedures of ASTM E519/E519M − 21 [32] or RILEM LUM B6 [33]. In some instances, research included even in situ tests of historical and heritage buildings [34]. The most commonly used reinforcement meshes are made of glass fibers [15,17,18,20,22,25,26,29] and, to a lesser extent, steel [20,21,24,28,30,31], basalt [19,21,27,28,31], carbon [16,23,30] or aramid [31]. The TRMs are generally arranged continuously over the entire surface of the panel, although the effect of discontinuous reinforcements has also been studied [21,24,28,31]. Another interesting aspect is the analysis of reinforcements applied only on one side of the walls, a frequent situation in the case of party walls or protected facades, for example, where it is not possible to intervene on both sides [15,17,19,20,25–27,29,30]. Furthermore, the effect of the installation of mechanical anchors to prevent possible debonding problems between the TRM and the supporting substrate has been evaluated in some studies [17,18,20–22,27,30,31]. To briefly summarize all these investigations, the following conclusions are worth highlighting: (i) TRM reinforcements significantly improve the response of masonry walls to in-plane loads, providing significant increases in strength and ductility; (ii) the stress-strain curves normally present an initial branch up to the failure of the substrate and mortar matrix, followed by a post-peak phase usually governed by the mechanical properties of the fibers used; (iii) generally, the original stiffness of the walls is not substantially altered by the effect of the TRM, an aspect of vital relevance in the case of seismic reinforcement of existing buildings; (iv) in almost all published studies, no debonding was observed between the TRM and the masonry substrates, even in the absence of connecting elements, demonstrating a high bonding capacity between the two materials; (v) the results confirm marked losses in efficiency in the case of single-sided strengthening, as the walls ended up deforming out of plane, so that it is in these situations that mechanical anchors might prove convenient to ensure that the two materials worked properly together. It is important to emphasize that these conclusions refer to walls analyzed under static diagonal compression; however, in other circumstances such as cyclic shear-compression tests, the detachment of TRM at substrate-to-matrix interface has been observed. In such cases, connectors may be necessary to ensure that the masonry and TRM work together properly [35].

In terms of the behavior of TRM reinforcements under elevated temperatures, the studies currently available are limited [36,37]. Inorganic mortars offer better performance than epoxy resins in FRPs, which are extremely vulnerable to heat. For this reason, these systems are often misperceived as fire resistant and therefore can be used without protection, when in fact this is not the case. In recent years, some published studies analyze the loss of mechanical properties of different TRMs exposed to elevated temperatures by means of uniaxial tensile coupon tests [38–42], or study their bonding to masonry or concrete substrates [43–47]. In this regard, it is fitting to note the study reported in Ref. [48], recently published by the authors of this research, in which an analysis was made of the tensile behavior of 4 different TRMs with glass, carbon and basalt fiber meshes (2 of which are the same as those used in the present work), exposed to temperature levels up to 600 °C. The main conclusions derived from this study are as follows: (i) at moderate temperature levels (up to 200 °C), TRMs retained their mechanical properties relatively intact; in fact, in some cases, increases in strength were observed which were attributed, on the one hand, to the shrinkage of the mortar matrix during the cooling process, improving adhesion with the fibers; on the other hand, in polymer-coated meshes, fiber-mortar bonding was increased as the coating softened under the effect of the heat; (ii) at 400 °C, significant strength losses were registered and, among all the materials studied, only the TRMs with carbon fibers seemed to retain part of their mechanical properties; (iii) at 600 °C, all the TRMs analyzed were seriously damaged and completely lost their mechanical capacity; the meshes were totally degraded and the fiber-mortar bonding was lost. In general, the results were consistent with those reported in previous investigations with TRMs subjected to elevated temperatures.

The purpose of this work is to analyze the shear behavior of masonry elements strengthened with TRM and subjected to high temperatures since, despite all the scientific production available to date, there is a significant lack of research in this area and there is hardly any published reference on the subject. For this purpose, panels formed by two layers of solid ceramic bricks and continuous reinforcements with glass or carbon fiber mesh, applied on both sides, are used. An exposure target temperature of 600 °C is adopted, which is chosen for two main reasons: (i) it is the usual temperature range that can occur during a fire inside a building with stone or masonry walls [49,50]; (ii) it has been shown that the mechanical capacity of the TRMs used is seriously compromised at this temperature level [48], which is why it is considered appropriate to evaluate the capacity of the reinforcements under these conditions. For the application of the TRMs, different scenarios are considered, so that the reinforcements are placed both after the exposure of the walls to 600 °C (i.e., panels with undamaged TRM) or before (elevated temperatures affecting both TRM reinforcement and masonry element). In this way, it is possible to simulate in the laboratory two different scenarios that might occur in a real situation: on the one hand, the hypothesis of a building whose walls are reinforced after having suffered a fire; on the other hand, the effect that a fire event could produce in a previously reinforced building, whereby the TRM would also be damaged by the fire. The results are then compared with those of equivalent series of unreinforced panels (at room temperature or subjected to 600 °C) or reinforced and tested at room temperature. Finally, the experimentally obtained data are compared to predictions from available design guides, which at the moment are limited to the North American ACI 549.6R-2020 [51] and the Italian CNR-DT 215/2018 [52]. Thus, the aim is to evaluate the level of accuracy that the analytical methods included in these standards may provide considering the conditions imposed by a high-temperature scenario.

2. Materials and methods

The experimental phase of this research program was conducted at the Large Structures Laboratory of the Civil Engineering Department of the University of Alicante (Spain). This section describes the properties of the materials used, the design of the experimental program and the test procedures.

2.1. Characterization of materials

For the construction of the panels covered by this study, solid clay bricks of dimensions 230 × 110 × 50 mm^3 were used, with a density of 1550 kg/m^3 and a compressive strength of 15 MPa, according to data provided by the manufacturer. The mortar used for the joints was a natural hydraulic lime mortar with pozzolan, with a density of 2000 kg/m^3 and a minimum compressive strength of 7.5 MPa, as declared by the supplier. However, the mechanical properties of both materials were also obtained experimentally. For this purpose, six brick samples of 110 × 110 × 50 mm^3 were prepared and tested in compression according to UNE-EN 772–1:2011 + A1:2016 [53], whereas another six brick specimens of 230 × 50 × 50 mm^3 were tested in flexural tension according to UNE-EN 772–6:2002 [54] and UNE-EN 1015–11:2020 [55]. Regarding the bed-joint mortar, three specimens of 160 × 40 × 40 mm^3 were manufactured and tested in flexural tension, and the compressive strength of the six resulting halves was subsequently obtained [51].

In all cases, two series of specimens were prepared in the same way: the first series of samples was tested at room temperature, while the second one was tested after exposure to 600 °C and natural cooling back to room temperature. For this purpose, a programmable electric furnace was used in which the specimens remained for 2 h at the target temperature. The results obtained are summarized in Table 1, with the corresponding coefficients of variation in parentheses. It is observed that the bricks suffer a loss in strength of 5% (in compression) and 17% (in bending), while the mortar is much more affected after exposure to 600 °C, with losses of 32% (in compression) and 58% (in bending). Table 1 also includes the compressive strength experimentally determined in prismatic masonry wallets of 710 × 540 × 230 mm^3 manufactured with the same materials and tested at room temperature, according to studies previously reported by the authors of this research [8].

Two different solutions were used for TRM strengthening of masonry. The first one (hereinafter referred to as "G") consisted of a polymer-coated glass fiber mesh, with a ready-mixed mortar made from natural hydraulic lime, reactive inorganic compounds, natural sand, special admixtures and micro-fibers. The second one (hereinafter referred to as "C") was an uncoated high-strength carbon fiber mesh, with a two-component fiber-reinforced mortar composed by hydraulic lime, Eco-Pozzolan, natural sand, special additives and synthetic polymers in water dispersion. A detail of both meshes is shown in Fig. 1, while Table 2 reports the most relevant properties of the materials, as stated by the supplier.

As mentioned in Section 1, the analysis of the TRM used had been previously reported by the authors in Ref. [48], which also includes other types of glass fiber and basalt fiber meshes. In this work, the behavior of TRM coupons tested to uniaxial tension according to the guidelines AC434 [56] and RILEM TC 232-TDT [57] is analyzed experimentally. To study the effect of the exposure of these materials to elevated temperatures, the coupons are divided into different series and exposed to 20, 100, 200, 400 and 600 °C, thereby observing the loss of mechanical properties with increasing temperature. Although the results obtained can be consulted in detail in the aforementioned reference, it is considered appropriate to summarize in Table 3 the data corresponding to the TRMs used in the present investigation, under the same temperature levels: A20 and A600 (coupons with glass fiber meshes at 20 and 600 °C) and C20 and C600 (coupons with carbon fiber meshes at 20 and 600 °C). Table 3 includes the following data: stress (σ_{cr}) and strain (ε_{cr}) at the cracking point of the mortar matrix; modulus of elasticity of the uncracked TRM (E_1); stress (σ_u) and strain (ε_u) at failure; and modulus of elasticity of the cracked TRM (E_3). These results are the average values of the 4 specimens in each set and the stresses and elastic moduli are referred to the area of the fibers, according to data provided by the supplier (Table 2). The cited reference [48] includes an Appendix with the stress-strain curves for all the series tested, showing the mean values and the bilateral 90% confidence intervals, to facilitate the visualization of the dispersions obtained in each set and each phase of the test.

On the other hand, and considering the present research scope, it is considered appropriate to highlight some important conclusions derived from Ref. [48]. Firstly, the behavior of TRM under high temperature exposure is closely related to the characteristics of the textiles used. At moderate temperatures (up to 200 °C) the effect of heat on the coating polymer of the glass fiber mesh improves the bond between the fibers and the mortar matrix, increasing the mechanical capacity of the material; however, at temperatures above 400 °C, the coating decomposes and the fibers become completely loose inside the matrix, losing completely the adhesion between both. This is not the case with carbon fiber meshes, which do not include such coating, finding that TRM partially retains its properties up to 400 °C (although it degrades completely at 600 °C). Secondly, the different nature of the matrices used has also a very important influence under the effect of elevated temperatures. In this regard, the presence of synthetic polymers and polypropylene fibers in the C matrix seems to have a negative effect at temperatures above 400 °C, while the G matrix shows a better behavior.

2.2. Experimental program and temperature exposure

For the experimental program of this study, 24 masonry panels of dimensions 610 × 610 × 230 mm^3 were prepared, formed by two layers of solid brick in stretched bond. The dimensions of the panels were limited by the size of the furnace available for exposure to elevated temperatures, as will be detailed later on. Each of the masonry specimens consisted of 10 rows of bricks and 15 mm thick mortar joints (approximately), with only the end pieces arranged as transversal connection between both layers. In this way, it was

Table 1
Mechanical properties of clay bricks, bed-joint mortar and masonry wallets (coefficient of variation in brackets).

	Compressive strength (MPa)		Flexural strength (MPa)	
	at 20 °C	at 600 °C	at 20 °C	at 600 °C
Clay bricks	13.9 (10%)	13.2 (9%)	4.2 (17%)	3.5 (12%)
Bed-joint mortar	8.4 (9%)	5.7 (5%)	1.2 (14%)	0.5 (4%)
Masonry wallets	4.9 (5%)	–	–	–

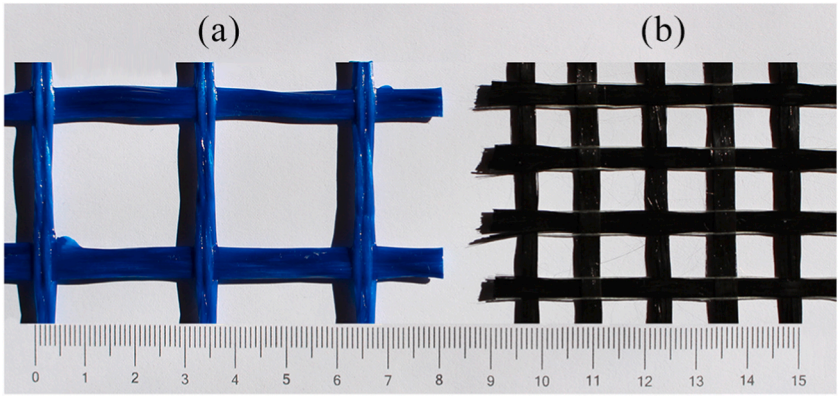

Fig. 1. Detail of glass (a) and carbon (b) fiber meshes.

Table 2
Properties of textiles and mortars used as TRM (values provided by the manufacturer).

TRM	G (glass fiber mesh)		C (carbon fiber mesh)	
	Textile	Matrix	Textile	Matrix
Mesh size (mm)	30 × 30	–	10 × 10	–
Weight (g/m^2)	420	–	170	–
Equivalent thickness of dry fabric (mm)	0.056	–	0.048	–
Tensile strength (kN/m)	105.6	–	240	–
Elongation at failure (%)	4	–	2	–
Modulus of elasticity (GPa)	33	10	252	8
Compressive strength (MPa)	–	>15	–	>15

Table 3
Experimental results on TRM tensile tests.

Set	σ_{cr} (MPa)	ε_{cr} (%)	E_1 (GPa)	σ_u (MPa)	ε_u (%)	E_3 (GPa)
A20	128	0.056	428	413	2.050	27.2
A600	61	0.016	190	64	0.121	0
C20	375	0.067	1104	1174	0.867	111.4
C600	48	0.063	120	48	0.063	0

intended to reproduce in the laboratory one of the most common construction solutions in buildings with brick masonry walls. The panels were cured in ambient laboratory conditions for 60 days before applying the TRM.

The strengthening with TRM started with the preparation of the panel surfaces by removing joint mortar residues, dust and dirt by means of a steel brush and compressed air. Next, a first layer of mortar about 5–6 mm thick was applied to the previously moistened surfaces of the specimens. With the mortar still fresh, the reinforcing mesh was placed, applying a slight pressure and making sure that the fiber strands were perfectly oriented in the horizontal and vertical directions of the panel. The dimensions of the specimens and meshes allowed the reinforcements to be placed in a continuous manner, without the need for intermediate overlaps. In all cases, a single mesh layer was placed on both sides of the panel. Among the two meshes used, only the carbon fiber one had been pre-impregnated with the liquid phase of the bi-component mortar, so as to increase bonding and following the manufacturer's recommendations (the fiberglass mesh was coated as supplied and did not require such pre-impregnation). The reinforcement process concluded with a second layer of mortar 5–6 mm thick and smoothing with a smooth-edged metal trowel, so that the total thickness of the TRM applied was around 10–12 mm. Once the reinforcements were finished, the walls were protected with polyethylene sheets to preserve humidity, which were kept for 7 days. The failure tests were carried out 60 days after the placement of the TRM in all cases. Fig. 2 shows a detail of the panels, with the brick arrangement and the strengthening process.

The experimental campaign is organized on the basis of 8 series and 3 specimens per series, with the encoding specified in Table 4. The first letter describes the strengthening solution adopted: N (none), G (glass fiber mesh) or C (carbon fiber mesh); this is followed by the exposure temperature: 20 or 600 °C; finally, in the case of reinforced panels exposed to 600 °C, a suffix is added: a (for reinforcements applied after exposure to high temperature, i.e. panels with undamaged TRM) or b (for reinforcements applied prior to exposure to the temperature, i.e. panels with heat-damaged TRM). In this way, and as previously mentioned, two different scenarios that could occur in a real building are simulated: on the one hand, the hypothesis of a strengthened building after having suffered a fire is considered; and on the other hand, the effect that a fire could have on a previously strengthened building, whereby the TRM would be damaged by the fire, is also evaluated.

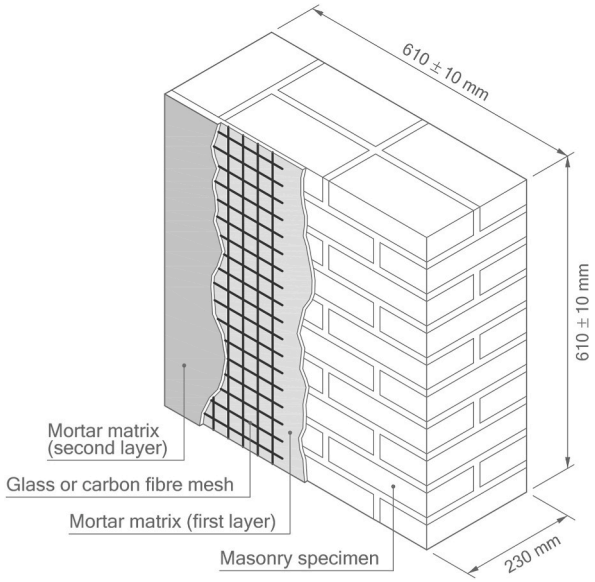

Fig. 2. Detail of masonry panel and TRM application process.

Table 4
Summary of experimental campaign and specimen designation.

ID	TRM	Temperature (°C)	Strengthening application	Samples
N20	–	20	–	3
N600		600		3
G20	Glass	20	At room temperature (TRM undamaged)	3
C20	Carbon	20		3
G600a	Glass	600	After temperature exposure (TRM undamaged)	3
C600a	Carbon	600		3
G600b	Glass	600	Before temperature exposure (TRM damaged)	3
C600b	Carbon	600		3
Total samples				24

The masonry specimens to be exposed at elevated temperature were placed inside a programmable electric furnace of clear internal dimensions 720 × 940 × 670 mm^3 (width × height × depth). These parameters had affected the size of the samples, as mentioned above. The furnace was programmed with an increasing heating rate of 5 °C/min, so that the target temperature was reached in 2 h, remaining constant for an additional 3 h. After this point, the oven was switched off and the panels remained inside for 24 h until reaching the ambient temperature of the laboratory. As an additional temperature monitorization, two thermocouples were installed in one of the N600 series panels and connected to a data acquisition equipment: one of the thermocouples was attached to the outer surface of the panel, thus measuring the air temperature inside the furnace; the second thermocouple was inserted into the center of gravity of the panel through a 3 mm diameter, 115 mm deep borehole, which was subsequently sealed with refractory mastic with a

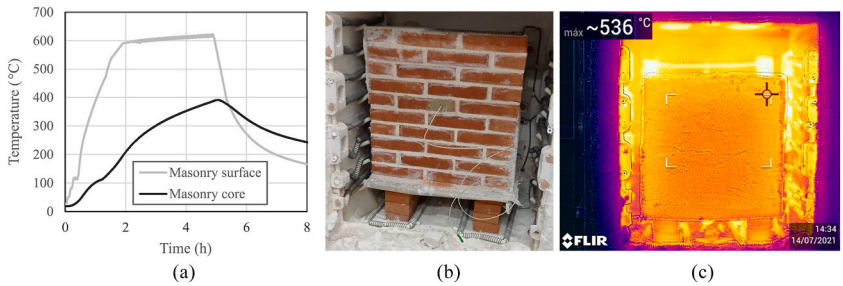

Fig. 3. High temperature exposure in masonry panels: (a) heating curves provided by thermocouples; (b) detail of a panel inside the oven; (c) temperature measurement by thermographic camera.

1200 °C temperature rating. Fig. 3a shows the time-temperature curves registered by both thermocouples, showing that although the target temperature of 600 °C was reached and maintained, the core of the panel did not exceed about 400 °C. A view of the N600 series panel placed inside the furnace with the thermocouple installed in its core is shown in Fig. 3b. Unlike the masonry, and owing to the narrower thickness, the TRM was able to reach approximately the target temperature of 600 °C and it is illustrated in Fig. 3c with an image taken with a thermographic camera on one of the C600a series panels, for which the furnace door was opened for a brief moment (logically, the air flow generated when the door was opened caused the temperature recorded by the camera to be lower than the one measured by the thermocouple).

2.3. Test setup and instrumentation

The panels were tested in diagonal compression—ultimate collapse induced by diagonal tension—, arranged vertically and rotated at 45°, according to ASTM E519/E519M − 21 [32]. A hydraulic press equipped with a 700 kN load cell was used for this purpose. The specimens were placed between two loading shoes made of 10 mm thick welded steel plates. To improve the contact between the masonry and the loading shoes, the bearing surfaces had been previously regularized with cement mortar and intermediate 5 mm thick neoprene sheets were installed, with a hardness level of 55 on the Shore A scale. In all cases, the tests were carried out by displacement control, at a constant rate of 0.01 mm/s.

For strain monitoring, the panels were instrumented in two different ways. Two LVDTs oriented along the two diagonals were installed on one of the faces, so that the horizontal LVDT provided the elongation in the X direction while the vertical LVDT registered the shortening in the Y direction, parallel to the load application. The gage length was 400 mm in both LVTDs. The deformations were recorded using an HBK QuantumX MX1615B data acquisition system, programmed at a sampling rate of 1 Hz. On the other hand, the opposite surface was monitored using Digital Image Correlation (DIC), employing a camera with a resolution of 16 MP placed at a distance of 1.8 m from the panel and programmed to shoot at a frequency of 0.1 Hz (i.e., one image every 10 s). The surface of the panels had been sprayed with a speckle pattern to enhance image contrast and the following analysis process, which was carried out using GOM Correlate software. A front and side schematic of the test setup is shown in Fig. 4a. A view of one of the reinforced panels and the arrangement of the two LVDTs is shown in Fig. 4b. Finally, a detail of the instrumentation for the DIC analysis on the opposite side of the panel can be seen in Fig. 4c.

3. Results

This section presents the results obtained in the diagonal compression tests and explains in detail the methodology adopted for the calculation of the strength, stiffness and ductility of the series studied. Also shown are the different modes of failure observed, which depend largely on the temperature level and the sequence of execution of the reinforcements (before or after heat treatment). The analysis and discussion of these results will be carried out in Section 4.

3.1. Shear stress-strain behavior

Calculation of the shear stresses and strains follows the criteria established in ASTM E519/E519M − 21 [32], although the notation has been modified in some aspects to match that of the design guidelines that will be discussed in the following section. The shear stress (τ) is obtained from Eq. (1), where V is the applied load and A_n represents the net area of the masonry specimen, which is determined

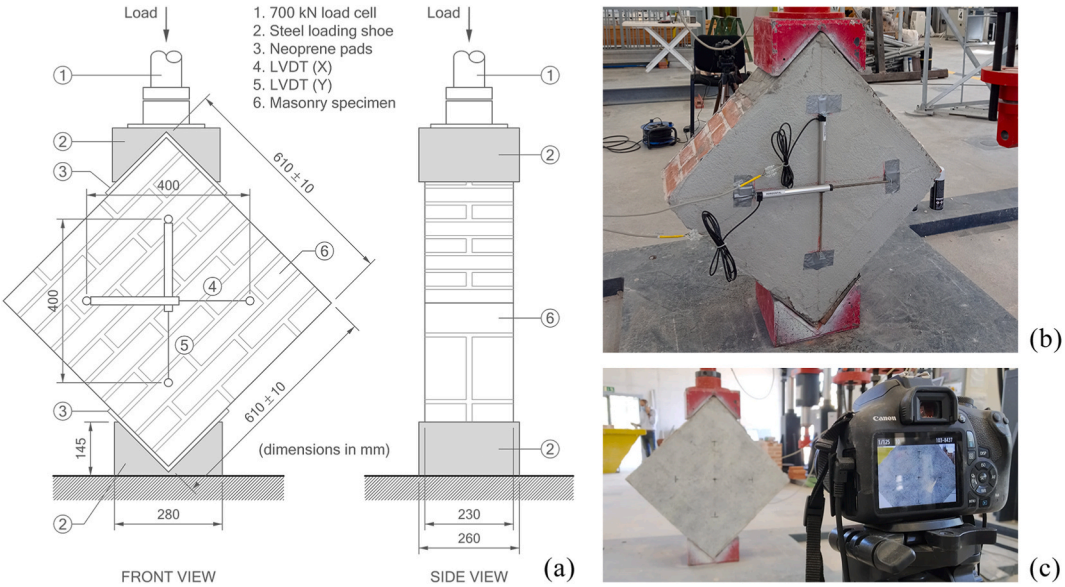

Fig. 4. Test set-up: (a) schematic view; (b) LVDTs arrangement; (c) DIC instrumentation.

through Eq. (2), where w and h are the width and height of the panel (in this case both dimensions are the same and equal to 610 mm), t is the thickness (230 mm) and n represents the percentage of solid pieces with respect to the total (in this case 1 as they are solid bricks).

$$\tau = \frac{0.707 \cdot V}{A_n} \tag{1}$$

$$A_n = \left(\frac{w+h}{2}\right) \cdot t \cdot n \tag{2}$$

Shear strains (γ) may be calculated through Eq. (3), where Δy and Δx are, respectively, the shortening along the direction parallel to the load and the extension along the orthogonal direction (absolute value), whilst g is the gauge length of the LVDTs (400 mm, as illustrated in Fig. 4).

$$\gamma = \frac{\Delta y + \Delta x}{g} \tag{3}$$

Finally, the modulus of rigidity (G) is determined as the ratio of shear stress to shear strain, through Eq. (4):

$$G = \frac{\tau}{\gamma} \tag{4}$$

As explained in Section 2, two LVDTs were installed on one side of the panel to register the deformations, while the opposite side was monitored by Digital Image Correlation (DIC). As will be explained later, the collapses of some specimens were sudden and brittle in nature. This resulted in the LVDTs having to be removed in the later stages of the test to avoid damaging them and, consequently, insufficient information was registered for a complete plotting of the stress-strain curves. For this reason, most of the curves presented in this section have been obtained from the data provided by the DIC, after verifying adequate calibration with LVDT measurements during the initial phase. This makes it possible to capture the deformations of the complete test up to failure, as has been successfully proven in previous works [29].

A reference curve is shown in Fig. 5 to identify the fundamental parameters of the test and to explain the adopted nomenclature. The modulus of rigidity (G) is determined in the elastic range as the secant modulus between the origin and a stress level of 30% with respect to the maximum [58]. In general, three reference points are controlled: point A corresponds to the maximum stress value recorded on the panel (τ_{max}), while points B and C enable the evaluation of the ductility factor (μ) as the ratio between ultimate (γ_u) and yield (γ_y) strains (some authors refer to this ratio as pseudo-ductility). In the calculation of γ_u, point B is defined as the maximum strain recorded during the test or, in curves showing a descending branch after the maximum stress peak, it is set at a stress drop of 20% ($0.8\tau_{max}$), following the criterion commonly accepted by most researchers. Regarding the calculation of γ_y there is no clear consensus in the different published studies: some authors associate this deformation with τ_{max} [15,27] or with a level of $0.7\tau_{max}$ [23–25], while other studies rely on simplified bilinear diagrams [17,19]. In this paper, γ_y is determined by means of point C, as the intersection between the straight lines associated with the maximum stress and the modulus of rigidity [18,28].

The shear stress-strain curves for all the series tested are presented in Fig. 6: unreinforced panels (Fig. 6a); reinforced panels at room temperature (Fig. 6b); reinforced panels subjected to 600 °C with the TRM undamaged (Fig. 6c); and reinforced panels subjected to 600 °C with the TRM damaged (Fig. 6d). In all cases, the results of the three specimens that make up each series are represented except for specimen G600b_3, for which reliable data are not available due to a data recording error. Note that the curves are plotted up to the last point recorded during the tests or up to a maximum shear strain value of 2%, where the shear stress drops exceed 20% in all cases

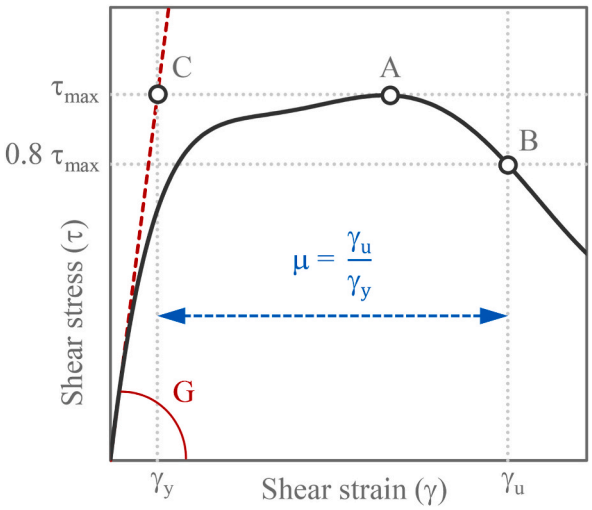

Fig. 5. Reference shear stress-strain curve for nomenclature definition.

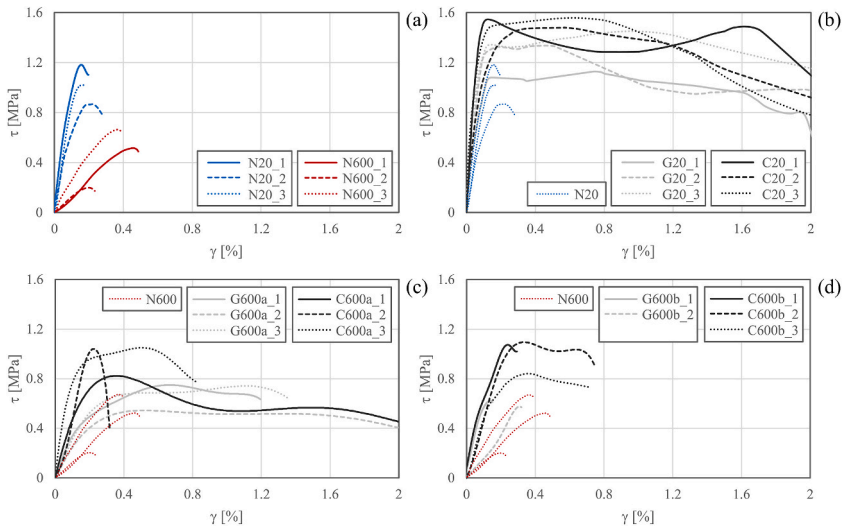

Fig. 6. Shear stress-strain curves: (a) unreinforced panels; (b) reinforced panels at room temperature; (c) reinforced panels at 600 °C, TRM undamaged; (d) reinforced panels at 600 °C, TRM damaged.

and point B can be identified without problems. The results of the tests are summarized in Table 5, which provides the individual data for each specimen and the average values of maximum shear stress, modulus of rigidity and ductility factor, as defined above. The corresponding coefficients of variation are also given in brackets, in order to evaluate the dispersions obtained.

It can be observed that the unreinforced panels exhibited an approximately linear behavior, with brittle failures (Fig. 6a). The results presented good repeatability except in the case of specimen N600_2, which was not considered for the calculation of the mean values. Exposure to 600 °C produced a notable loss of mechanical properties, with decreases in strength and stiffness of 43% and 79%, respectively. These decreases are mainly attributed to the reduction in the strength of the mortar joint (Table 1) and to the deterioration of the bond at the brick-mortar interface due to the effect of temperature. It is therefore quite apparent that the action of a fire in a building with masonry walls might have a significant negative effect on the capacity of these walls to withstand in-plane stresses.

Table 5
Summary of diagonal compression test results (coefficients of variation in brackets).

ID	V_{max} (kN)	τ_{max} (MPa)	Average τ_{max} (MPa)	G (MPa)	Average G (MPa)	γ_y (%)	γ_u (%)	μ	Average μ
N20_1	238	1.20	**1.03** (16%)	973	**882** (11%)	0.12	0.17	1.42	**1.73** (23%)
N20_2	173	0.87		785		0.11	0.24	2.18	
N20_3	204	1.03		889		0.12	0.19	1.58	
N600_1	101	0.51	**0.59**[a] (18%)	139	**182**[a] (33%)	0.37	0.49	1.32	**1.33**[a] (1%)
N600_2	38	0.19		111		0.17	0.23	1.35	
N600_3	131	0.66		224		0.29	0.39	1.34	
G20_1	224	1.13	**1.31** (12%)	1371	**1595** (14%)	0.08	1.69	21.13	**18.61** (18%)
G20_2	266	1.34		1820		0.07	1.03	14.71	
G20_3	288	1.45		1593		0.09	1.80	20.00	
C20_1	308	1.55	**1.53** (3%)	2092	**1859** (11%)	0.07	1.88	26.86	**19.03** (36%)
C20_2	294	1.48		1677		0.09	1.41	15.67	
C20_3	310	1.56		1808		0.09	1.31	14.56	
G600a_1	147	0.74	**0.69** (13%)	351	**343** (11%)	0.21	1.19	5.67	**7.17** (24%)
G600a_2	115	0.58		302		0.19	1.72	9.05	
G600a_3	147	0.74		375		0.20	1.36	6.80	
C600a_1	167	0.84	**0.98** (12%)	670	**763** (25%)	0.12	0.67	5.58	**4.78** (57%)
C600a_2	208	1.05		638		0.16	0.28	1.75	
C600a_3	206	1.04		980		0.11	0.77	7.00	
G600b_1	125	0.63	**0.61** (6%)	517	**387** (48%)	0.12	0.18	1.50	**1.47** (3%)
G600b_2	115	0.58		256		0.23	0.33	1.43	
G600b_3[b]	–	–		–		–	–	–	
C600b_1	218	1.10	**1.00** (14%)	656	**578** (12%)	0.17	0.30	1.76	**3.44** (45%)
C600b_2	212	1.07		533		0.20	0.75	3.75	
C600b_3	167	0.84		545		0.15	0.72	4.80	

[a] The specimen N600_2 is not considered in the averages.
[b] No reliable data for specimen G600b_3.

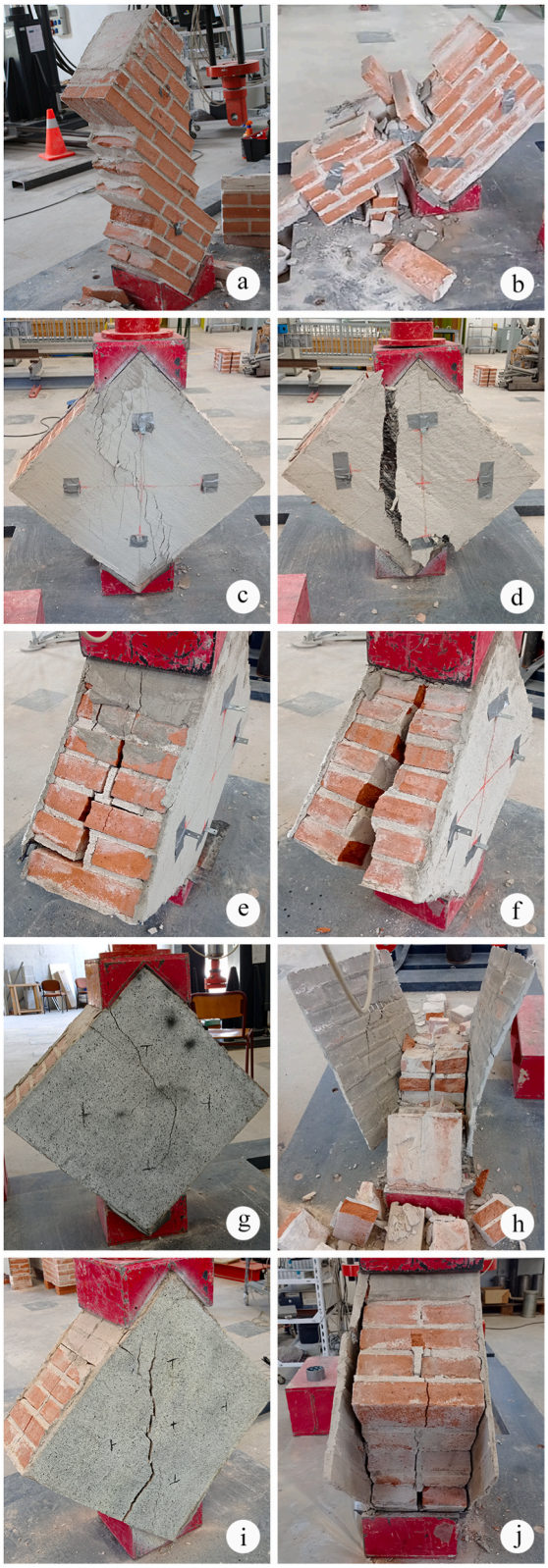

Fig. 7. Examples of failure modes in the different series tested: (a) N20; (b) N600; (c) G20; (d) C20; (e) G600a; (f) C600a; (g–h) G600b; (i–j) C600b.

Regarding the strengthened series tested at room temperature, the results are consistent with those reported in most of the previous investigations referenced in Section 1. It was observed that the reinforcements provided an increase in strength of about 26% (G20) and 48% (C20). Moreover, there was also a clear increase in stiffness with respect to the unreinforced panels, with gains of 81% (G20) and 111% (C20), approximately. As is often reported, carbon fiber reinforcements provide the best results, owing to the mechanical properties of the meshes used (Table 2). However, the main benefit of TRM on the panels studied is undoubtedly the ductility provided. As shown in Fig. 6b, the shear stress-strain curves presented a substantial post-peak phase, in line with the diagrams reported in most of the available literature. Regarding the ductility factor obtained, it is remarkable to observe the similarity between the two series tested (18.61 in G20 and 19.03 in C20), regardless of the different properties of the TRMs used. Finally, it is worth noting the good homogeneity that these series also showed, and only in the case of specimen C20_1 a somewhat different behavior is observed, with a slight hardening in the post-peak phase that was not detected in the rest of the panels tested.

The strengthened panels subjected to 600 °C behaved distinctly differently depending on the type of fibers used and the order of application of the TRM (before or after exposure to the temperature). In the case of the specimens with undamaged TRM (Fig. 6c), the transition between the first and second branches of the shear stress-strain curves was smoother and did not produce a point as marked as in the panels tested at room temperature. In general, a remarkable post-peak phase with large ultimate deformations was obtained, except in the case of specimen C600a_2, where a brittle rupture occurred. Although the results will be discussed in more detail in Section 4, it should be noted here that carbon fiber reinforcements practically restored the strength and stiffness of the original panels (N20), which was not possible with glass fibers. At the same time, in the series with damaged TRM (Fig. 6d), it can be seen how the carbon fiber reinforcements also practically restored the original strength and stiffness (just as in the previous case), although the ductility provided was lower. However, the glass fiber reinforcements seemed to lose all their mechanical capacity and the panels behaved as if they had not been reinforced at all (N600). In this sense, it is interesting to contrast these results with the uniaxial tensile tests on TRM coupons made with the same materials and exposed to the same temperatures [48], summarized in Table 3, as will be discussed in Section 4.

3.2. Crack patterns and failure modes

To analyze the cracking and failure modes, Fig. 7 shows some representative images of the different series tested. Unreinforced panels presented a brittle failure, with cracking lines in the direction of the compressed diagonal and in a stair-stepped cracking pattern, following the head and bed mortar joints. Exceptionally, some of the bricks did indeed crack, as can be seen in Fig. 7a. The failure mode was similar both in the panels tested at room temperature and those subjected to 600 °C, although in the first case the walls retained a certain integrity after the collapse, while in the second case the masonry was generally more heavily damaged, as can be seen in Fig. 7b.

The failure mode of reinforced masonry specimens tested at room temperature changed drastically. In the first phase of the test, no damage was detected visually until approximately 80–90% of the maximum shear stress had been reached. From this point on, very thin cracks appeared along the compressed diagonal, which gradually developed as the displacements increased and the post-peak phase (explained in the previous section) unfolded. This intermediate cracking state can be observed in Fig. 7c for one of the specimens of the G20 series. In the later stages of the test, a main crack typically grew and progressed rapidly until the panel failed, as shown in Fig. 7d, which corresponds to a specimen of the C20 series. Ultimate failure of the TRM was caused by slippage of the fibers with respect to the mortar matrix, and no tensile fiber breaks were observed in any case. In general, the failure modes were similar in both series (carbon and glass), and no significant differences were observed regardless of the different reinforcement meshes used. On the other hand, it is important to highlight that no debonding was produced between the TRM and the brick substrate in any of the specimens tested, which shows the high bonding capacity between the two materials.

The panels exposed to 600 °C with the TRM undamaged exhibited a very different behavior. The response of the two meshes used was the same, with the TRM remaining practically intact throughout the test, as can be seen in Fig. 7e (G600a) and Fig. 7f (C600a). The failure was caused by the degradation of the masonry core, as a consequence of the loss of bond between the bricks and the bed joint mortar. Collapse occurred in a ductile mode and took place slowly with increasing displacements, resulting in the post-peak phase that can be seen in Fig. 6c. A different type of failure was observed only in the case of specimen C600a_2, with a brittle rupture through the midplane of the panel and a complete separation of the 2 brick layers (Fig. 7f). In addition, it was again found that no debonding of the TRM had occurred in any of the tested panels, which may demonstrate once again a remarkable bonding strength even on damaged substrates after exposure to elevated temperatures. In general, the failure modes obtained in these series were comparable to those reported in Ref. [23], where masonry cracking was observed in case of specimens with high reinforcement ratios (4 layers of carbon fiber mesh on each side).

Finally, and unlike in the previous cases, the behavior of the panels exposed to 600 °C with damaged TRM did indeed change depending on the meshes used. In the case of glass fibers, practically no appreciable damage was observed until the collapse of the masonry specimen, which occurred abruptly and without warning (Fig. 7g and h). The panels behaved essentially as if they were had not been reinforced at all: the brickwork was severely affected and the TRM underwent complete debonding, so it can be concluded that exposure to 600 °C completely canceled out the reinforcing capacity of the reinforcement. However, in the case of carbon fibers, the TRM was found to control part of the mechanical properties of the system. Similarly to what happened in the series tested at room temperature, the appearance of cracks along the direction of the compressed diagonal was again observed, with cracks progressing as the displacements increased (Fig. 7i). However, in this case the post-peak phase was briefer and in the last phase of the test there was a rapid slippage of the fibers with respect to the mortar matrix, the meshes having become strongly degraded due to the effect of the temperature. In the ultimate failures, a certain decomposition of the masonry core and partial debonding of the TRM were observed (Fig. 7j) but, in general, the panels retained their integrity.

4. Discussion

This section discusses the experimental results, focusing the analysis on the two fundamental hypotheses of this work: (i) reinforcements placed after the exposure of the panels to 600 °C (undamaged TRM), a situation that would represent the case of a building whose walls are reinforced after having undergone a fire; (ii) reinforcements placed before the exposure to the temperature (damaged TRM), in order to analyze the effect that a fire could have on a previously strengthened building. Finally, the experimentally obtained data are compared with the predictions of the available design guides.

4.1. Effect of high temperature on strengthened panels (undamaged TRM)

As explained in Section 3, the panels exposed to 600 °C with undamaged TRM exhibited a different behavior depending on the meshes used. In the case of carbon fibers, it was found that the reinforcements practically restored the mechanical capacity of the original walls (N20), both in terms of strength (0.98 vs. 1.03 MPa) and stiffness (763 vs. 882 MPa). In addition, the TRM provided additional ductility that the panels did not initially possess. However, the glass fiber meshes did not offer the same performance: in this case, the maximum stress (0.69 MPa) and the modulus of rigidity (343 MPa) were significantly lower, although the TRM still provided some substantial ductility that the original specimens lacked.

However, it is considered appropriate to compare the G600a and C600a series with respect to N600, in order to evaluate the capacity of the different TRMs over unreinforced damaged panels. On the other hand, another interesting comparison can be made between G20 - G600a and between C20 – C600a, to analyze the effectiveness of the undamaged reinforcements on healthy substrates or those affected by exposure to elevated temperatures. For this purpose, the increases in shear strength ($\Delta\tau_{max}$), transverse modulus (ΔG) and ductility ($\Delta\mu$) are calculated according to Eq. (5), particularized as an example for the case of the increase in the maximum shear stress of the G600a series with respect to N600.

$$\Delta\tau_{max} = \frac{\tau_{max,G600a} - \tau_{max,N600}}{\tau_{max,N600}} \times 100 \tag{5}$$

The results, in percentage, are graphically represented in Fig. 8, to allow a visual evaluation of the obtained increments in a simple way: $\Delta\tau_{max}$ (on the X axis), ΔG (on the y axis) and $\Delta\mu$ (inside the circles). As can be seen in Fig. 8a, TRMs with carbon fibers increased strength by 67% and especially stiffness by 320%, compared to the N600 series. In the case of glass fibers the increases were clearly lower (17% and 89% respectively). However, it was these fibers that provided the greatest increases in ductility (437% vs. 258%). When compared with the strengthened series at 20 °C (Fig. 8b), the G20 vs. G600a ratio presented the greatest increases (90% in strength and 365% in stiffness, compared to 57% and 144% obtained with carbon fibers), which would suggest that the glass fiber reinforcements appear to be more sensitive to the damage that the masonry substrate may have suffered due to by exposure to temperature. On the other hand, the opposite trend is observed in terms of ductility (159% vs. 298%). In general, the results obtained are consistent with the properties of the materials used (Table 3, sets A20 and C20): at room temperature, the TRMs with carbon fibers had the highest shear strength and stiffness, but the ultimate deformations using glass fibers were clearly superior.

4.2. Effect of high temperature on strengthened panels (damaged TRM)

In the panels exposed to 600 °C with the TRM damaged, the carbon fibers were once again able to restore the shear strength of the original walls (1.00 vs. 1.03 MPa), although in this case the stiffness did not seem to be fully recovered (578 vs. 882 MPa). The reinforcements still added ductility, although to a lesser extent than in the case of the specimens with the undamaged TRM. The fundamental difference stemmed from the glass fiber reinforcements, which were much more adversely affected by the temperature, so that the panels behaved almost as if they had not been strengthened, as mentioned above.

By comparing the G600b and C600b series with respect to N600 (Fig. 8a), it can again be seen that the carbon fiber reinforcements contributed the greatest increases in both shear strength (72%) and stiffness (219%), while the ratios with glass fibers were clearly lower (3% and 111%, respectively). It is important to note that the apparent increase in stiffness detected in the G600b series is not considered real, taking into account the failure of one of the specimens and the large dispersions obtained (Table 5). In terms of ductility, there was an increase of 158% with carbon fibers and practically no increase with glass fibers, given the brittle nature of the

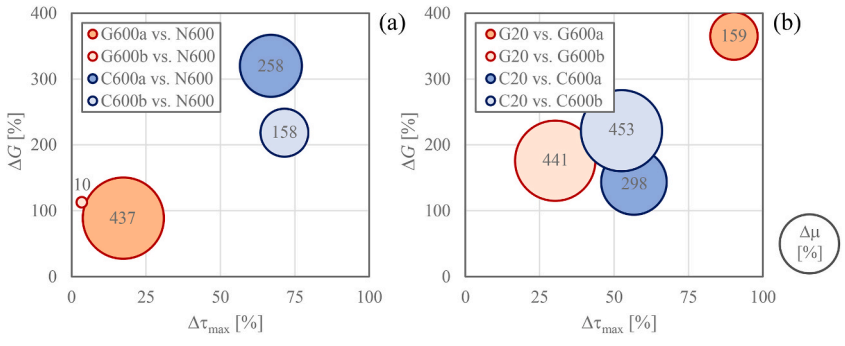

Fig. 8. Percentage increases computed for maximum shear stress ($\Delta\tau_{max}$, in x-axis), modulus of rigidity (ΔG, in y-axis) and ductility ratio ($\Delta\mu$, inside the circles).

failures in this series. The least marked differences were observed when comparisons were made with the equivalent series reinforced at 20 °C (Fig. 8b).

On the other hand, it is important to correlate the results obtained in the G600b and C600b series with the data of the TRM coupons exposed to 600 °C and tested in tension (Table 3, A600 and C600 sets). As explained in Section 2.1, both materials became seriously damaged by the temperature and lost almost all their mechanical capacity. The meshes were totally degraded and the fiber-mortar bonding was cancelled. Masonry specimens with glass fibers clearly reproduced this degradation and behave basically as if they had not been reinforced. However, TRMs with carbon fibers seemed to partially retain their mechanical capacity under these circumstances. One possible explanation for this phenomenon seems to lie in the conditions of exposure of the meshes to temperature: the coupons tested in tensile tests were thin pieces exposed on both sides, while the TRM adhered to the masonry substrate had only one of its sides exposed and was, therefore, better protected. In this regard, it is important to note that TRMs with carbon fibers retain part of their mechanical properties up to 400 °C, mainly because these meshes are uncoated and exhibit a better response at these temperature levels [48].

In addition, it is very important to highlight that the effect of high temperature has a decisive influence on the bond between TRM and masonry substrate. In Ref. [47] bond decreases around 50% are obtained in specimens exposed to 400 °C, studying TRMs with glass fiber textiles and four different matrices (two cement-based and two alkali-activated mortars). In Ref. [46] decreases between 61% and 74% are reported with carbon or basalt fiber meshes and cement or lime-based matrices, after exposure to 500 °C. In these works, the failure modes observed are basically tensile rupture or slippage of the fibers within the mortar matrix, but the failure due to delamination or debonding of the TRM is not reported in any case. Currently, the state-of-the-art about TRM-to-masonry bond is still very limited and very few studies have been published on this topic, so it will be interesting to specifically analyze this effect in future works.

Finally, it should be noted that the series with damaged TRMs were the only ones in which debonding between the reinforcements and the masonry substrate occurred. As explained in Section 1, the excellent bond strength between these materials normally makes the installation of connectors unnecessary, except in the case of one-sided reinforcements that may present out-of-plane deformations or walls subjected to cyclic shear-compression tests. However, in the particular case of exposure to elevated temperatures, connectors could prevent this phenomenon and possibly improve the strengthening capacity of TRMs. Further experimental studies will be necessary in the future to verify this aspect, as hardly any references on this topic are available at present.

4.3. Comparison with design guides

Finally, the experimentally obtained results are now contrasted in this section with the predictions of the available design guides. These are currently limited to the North American ACI 549.6R-2020 [51] and the Italian CNR-DT 215/2018 [52]. Some terms of the notation indicated in these guides have been modified, in order to homogenize the formulation between both documents and with other parameters defined throughout this article. It should be mentioned that the analytical methods defined in these guides are restricted to normal service conditions, so the main novelty of this study is assessing their potential application to an accidental situation with degradation of the mechanical properties of the materials.

The shear resistance of a reinforced wall (V_{rm}) strengthened with TRM can be calculated according to Eq. (6), as the sum of the resistance of the unreinforced wall (V_{urm}) and the contribution of the reinforcement (V_f).

$$V_{rm} = V_{urm} + V_f \tag{6}$$

To calculate the shear resistance of the unreinforced wall, the formulation of the design codes for masonry structures might be followed (e.g. Ref. [58]), or it might also be determined experimentally. In this work, the average values of V_{max} corresponding to the N20 or N600 series, as appropriate, are adopted (Table 5). Regarding the contribution of reinforcement, the formulations of ACI 549.6R-2020 and CNR-DT 215/2018 are presented respectively in Eqs. (7) and (8).

$$\text{ACI}: \ V_f = n_f \cdot A_f \cdot E_f \cdot \varepsilon_{fd} \tag{7}$$

$$\text{CNR}: V_f = \frac{1}{\gamma_{Rd}} \cdot n_f \cdot t_f \cdot l_f \cdot \alpha_t \cdot \varepsilon_{fd} \cdot E_f \tag{8}$$

In these expressions n_f is the number of layers of reinforcement applied (in this case 2); A_f is the total area of the reinforcement fibers in the direction parallel to the shear stress, equivalent to the product $t_f \cdot l_f$, where t_f is the equivalent thickness of the fibers provided by the manufacturer (Table 2) and l_f is the lateral dimension of the panel (610 mm); E_f is the modulus of elasticity of the TRM, which ACI assumes to be equal to the modulus in the cracked phase determined in the tensile TRM coupon tests (E_3 according to Table 3), while CNR directly adopts the elastic modulus of the dry textile (Table 2); γ_{Rd} is a partial safety coefficient (equal to 2 as defined by the Italian standard) that is not considered in this study for proper comparison of predictions with experimental results; α_t is an additional coefficient equal to 0.8 that the Italian standard establishes in a generic way, in absence of further experimental evidence; finally, ε_{fd} represents the design ultimate strain, which each of the guides approaches in a different way: while ACI imposes a limit of 0.004 for the calculations, CNR defines a conventional limit deformation ($\varepsilon_{lim,conv}$) that takes into account the different failure modes of the TRM. In this paper, the experimentally determined ε_u value is adopted in both cases (Table 3) without considering any conventional limitation.

Table 6 summarizes the results obtained, where V_{exp} represents the maximum load determined experimentally, according to the average value of the 3 specimens in each series (Table 5). Regarding V_f, it is important to highlight that in series G600b and C600b the value is null because, as explained in previous sections, the TRMs were completely degraded after exposure to 600 °C (Table 3). Note

that both guides provide a good level of approximation in all the series tested, in spite of the fact that the analytical expressions did not relate in principle to a situation involving mechanical degradation caused by exposure to high temperatures. As can be seen, a significant deviation is only observed in the case of C600b. This difference, as previously discussed, might be due to the fact that carbon fiber reinforcements seemed to retain part of their mechanical capacity in spite of temperature exposure; however, the analytical approach of the guides leaves out this circumstance by considering $E_f = 0$ (derived from the E_3 value in Table 3).

Finally, Fig. 9 plots the shear strength obtained experimentally, on the abscissa axis, versus those determined with the formulation of ACI 549.6R-2020 (Fig. 9a) or CNR-DT 215/2018 (Fig. 9b), on the ordinate axis. In these graphs, all the specimens tested are represented, to visually assess the resulting dispersions. In general terms, and leaving aside the case of the C600b series for the reason just explained, it is observed that both guides provide good results and only slight differences can be appreciated in the case of carbon fiber meshes. Taking into account the calculation hypotheses considered in this work, the only parameter that is different in the formulations of the two guides is E_f. Comparing the experimentally obtained values (E_3 in Table 3) with the data provided by the manufacturer for dry fabrics (Table 2), it can be seen that the results are very similar in the case of glass fibers (27 vs. 33 MPa), but show a greater deviation in the case of carbon fibers (111 vs. 252 MPa). Thus, it may be argued that the American standard tends to provide conservative values, whilst the Italian standard would seem to give results higher than those obtained experimentally. In this regard, it should not be forgotten that CNR-DT 215/2018 defines a partial safety coefficient (γ_{Rd}) that has not been considered in the calculations.

5. Conclusions

This study has experimentally examined the behavior of solid brick masonry panels subjected to in-plane stresses by means of diagonal compression tests. The panels were strengthened with TRM with glass or carbon fiber mesh and tested at room temperature or after being subjected to 600 °C. Reinforcements were applied after (undamaged TRM) or before (damaged TRM) exposure to temperature. In this way it was possible to simulate, in controlled laboratory conditions, different scenarios which would occur as a consequence of a fire in a real building. The principal conclusions derived from this work are as follows:

- Unreinforced panels exhibited an approximately linear response resulting in brittle collapses. Exposure to 600 °C produced significant drops in strength and stiffness, which were attributable essentially to the degradation of the mortar joint strength along with the loss of bond across the brick-mortar interface. Accordingly, it has been possible to experimentally assess the impact of a fire event on the capacity of masonry walls to withstand in-plane stresses.
- At room temperature, TRM strengthening clearly improved shear strength and stiffness of the masonry, but most importantly, it provided greater ductility, characterized by stress-strain curves with a pronounced post-peak phase and high ultimate strains. No debonding was observed between the reinforcement and the masonry substrate in any case, showing a high bonding capacity between both materials. In general, the results obtained were consistent with most of the previously published studies.
- In the specimens exposed to 600 °C with undamaged TRM (strengthened after temperature exposure), carbon fiber reinforcements practically restored the original capacity of the panels (i.e., room temperature without TRM) in terms of both strength and stiffness, but also providing greater ductility that the original panels did not possess. In contrast, reinforcements with glass fibers offer poorer performance, given the mechanical properties of the meshes used. In general, failures occurred as a result of the degradation of the masonry core, with the TRMs remaining practically intact throughout the tests, and without any debonding being observed in any of the specimens studied.
- In the specimens exposed to 600 °C with damaged TRM (strengthened before temperature exposure), carbon fibers were once again able to restore the original strength of the panels, although the stiffness did not seem to be fully recovered. The reinforcements were still providing ductility, but to a lesser extent. However, the TRMs with glass fibers were much more severely affected by temperature and the panels basically behaved as if they had not been strengthened. These series were the only ones in which debonding between the TRM and the brick substrate occurred, so further research should explore the installation of connectors to potentially prevent this phenomenon.
- The experimental results have been compared with analytical models from ACI 549.6R-2020 and CNR-DT 215/2018 design guides. Although they are not originally intended for use in applications involving materials exposed to high temperatures, both guides seem to provide generally a close estimation and the only deviation is observed in the case of panels with carbon fiber TRMs exposed to 600 °C. These reinforcements would appear to retain part of their mechanical capacity despite exposure to temperature. Nonetheless, the formulation of the guides does not consider this circumstance by adopting the data of TRM coupons tested in tension, tests in which the material was found to suffer an almost complete degradation at 600 °C, regardless of the fibers used.

Author statement

L. Estevan: Methodology, Formal analysis, Investigation, Visualization, Writing - Original Draft, **B. Torres:** Methodology, Formal analysis, Investigation, Visualization, Writing - Review & Editing, **F.B. Varona:** Conceptualization, Project administration, Funding acquisition, Writing - Review & Editing, **F.J. Baeza:** Conceptualization, Supervision, Investigation, Writing - Review & Editing, **S. Ivorra:** Supervision, Project administration, Funding acquisition, Writing - Review & Editing.

Declaration of competing interest

The authors declare that they have no known competing financial interests or personal relationships that could have appeared to

Table 6
Experimental results vs. design guides prediction.

ID	V_{exp} (kN)	V_{urm} (kN)	ACI 549.6R-2020			CNR-DT 215/2018		
			V_f (kN)	V_{rm} (kN)	V_{exp}/V_{rm}	V_f (kN)	V_{rm} (kN)	V_{exp}/V_{rm}
G20	259	205	38	243	1.07	37	242	1.07
C20	304	205	57	262	1.16	103	308	0.99
G600a	136	116	38	154	0.89	37	153	0.89
C600a	194	116	57	173	1.12	103	219	0.89
G600b	120	116	0	116	1.03	0	116	1.03
C600b	199	116	0	116	1.72	0	116	1.72

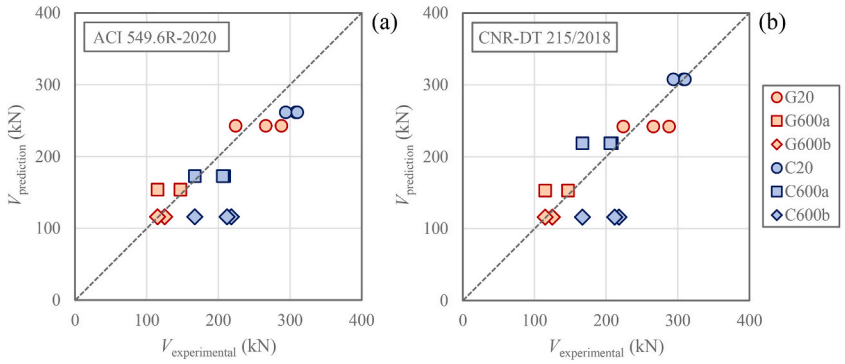

Fig. 9. Experimental results vs. design guides prediction: (a) ACI 549.6R-2020; (b) CNR-DT 215/2018.

influence the work reported in this paper.

Data availability

Data will be made available on request.

Acknowledgements

The authors would like to acknowledge Mapei Spain and Grupo Puma for the materials supplied in this work. This research has been funded by the Spanish Ministry of Science, Innovation and Universities, grant number RTI2018-101148-B-100.

Appendix A. Supplementary data

Supplementary data to this article can be found online at https://doi.org/10.1016/j.jobe.2022.105511.

References

[1] A. Penna, P. Morandi, M. Rota, C.F. Manzini, F. da Porto, G. Magenes, Performance of masonry buildings during the Emilia 2012 earthquake, Bull. Earthq. Eng. 12 (2014) 2255–2273, https://doi.org/10.1007/s10518-013-9496-6.
[2] L. Sorrentino, S. Cattari, F. da Porto, G. Magenes, A. Penna, Seismic behaviour of ordinary masonry buildings during the 2016 central Italy earthquakes, Bull. Earthq. Eng. 17 (2019) 5583–5607, https://doi.org/10.1007/s10518-018-0370-4.
[3] L.A.S. Kouris, T.C. Triantafillou, State-of-the-art on strengthening of masonry structures with textile reinforced mortar (TRM), Construct. Build. Mater. 188 (2018) 1221–1233, https://doi.org/10.1016/j.conbuildmat.2018.08.039.
[4] C.G. Papanicolaou, T.C. Triantafillou, M. Papathanasiou, K. Karlos, Textile reinforced mortar (TRM) versus FRP as strengthening material of URM walls: out-of-plane cyclic loading, Mater. Struct. Constr. 41 (2008) 143–157, https://doi.org/10.1617/s11527-007-9226-0.
[5] C.G. Papanicolaou, T.C. Triantafillou, K. Karlos, M. Papathanasiou, Textile-reinforced mortar (TRM) versus FRP as strengthening material of URM walls: in-plane cyclic loading, Mater. Struct. Constr. 40 (2007) 1081–1097, https://doi.org/10.1617/s11527-006-9207-8.
[6] E. Bernat, L. Gil, P. Roca, C. Escrig, Experimental and analytical study of TRM strengthened brickwork walls under eccentric compressive loading, Construct. Build. Mater. 44 (2013) 35–47, https://doi.org/10.1016/j.conbuildmat.2013.03.006.
[7] S. Ivorra, B. Torres, F.J. Baeza, D. Bru, In-plane shear cyclic behavior of windowed masonry walls reinforced with textile reinforced mortars, Eng. Struct. 226 (2021), 111343, https://doi.org/10.1016/j.engstruct.2020.111343.
[8] B. Torres, S. Ivorra, F. Javier Baeza, L. Estevan, B. Varona, Textile reinforced mortars (TRM) for repairing and retrofitting masonry walls subjected to in-plane cyclic loads, An experimental approach, Eng. Struct. 231 (2021), 111742, https://doi.org/10.1016/j.engstruct.2020.111742.
[9] L. Estevan, F.J. Baeza, D. Bru, S. Ivorra, Stone masonry confinement with FRP and FRCM composites, Construct. Build. Mater. 237 (2020), 117612, https://doi.org/10.1016/j.conbuildmat.2019.117612.
[10] A. Cascardi, F. Micelli, M.A. Aiello, FRCM-confined masonry columns: experimental investigation on the effect of the inorganic matrix properties, Construct. Build. Mater. 186 (2018) 811–825, https://doi.org/10.1016/j.conbuildmat.2018.08.020.

[11] F.A. Kariou, S.P. Triantafyllou, D.A. Bournas, TRM strengthening of masonry arches: an experimental investigation on the effect of strengthening layout and textile fibre material, Compos. B Eng. 173 (2019), 106765, https://doi.org/10.1016/j.compositesb.2019.04.026.
[12] E. Bertolesi, B. Torres, J.M. Adam, P.A. Calderón, J.J. Moragues, Effectiveness of Textile Reinforced Mortar (TRM) materials for the repair of full-scale timbrel masonry cross vaults, Eng. Struct. 220 (2020), 110978, https://doi.org/10.1016/j.engstruct.2020.110978.
[13] L. Mercedes, E. Bernat-Maso, L. Gil, In-plane cyclic loading of masonry walls strengthened by vegetal-fabric-reinforced cementitious matrix (FRCM) composites, Eng. Struct. 221 (2020), 111097, https://doi.org/10.1016/j.engstruct.2020.111097.
[14] T. Celano, L.U. Argiento, F. Ceroni, C. Casapulla, Literature Review of the in-plane behavior of masonry walls: theoretical vs, Exp.Results Mater. 14 (2021) 3063, https://doi.org/10.3390/ma14113063.
[15] A. Prota, G. Marcari, G. Fabbrocino, G. Manfredi, C. Aldea, Experimental in-plane behavior of tuff masonry strengthened with cementitious matrix-grid composites, J. Compos. Construct. 10 (2006) 223–233, https://doi.org/10.1061/(asce)1090-0268 (2006)10:3(223).
[16] C. Faella, E. Martinelli, E. Nigro, S. Paciello, Shear capacity of masonry walls externally strengthened by a cement-based composite material : an experimental campaign, Construct. Build. Mater. 24 (2010) 84–93, https://doi.org/10.1016/j.conbuildmat.2009.08.019.
[17] F. Parisi, I. Iovinella, A. Balsamo, N. Augenti, A. Prota, In-plane behaviour of tuff masonry strengthened with inorganic matrix-grid composites, Compos. B Eng. 45 (2013) 1657–1666, https://doi.org/10.1016/j.compositesb.2012.09.068.
[18] N. Gattesco, I. Boem, Experimental and analytical study to evaluate the effectiveness of an in-plane reinforcement for masonry walls using GFRP meshes, Construct. Build. Mater. 88 (2015) 94–104, https://doi.org/10.1016/j.conbuildmat.2015.04.014.
[19] G. Marcari, M. Basili, F. Vestroni, Experimental investigation of tuff masonry panels reinforced with surface bonded basalt textile-reinforced mortar, Compos. B Eng. 108 (2017) 131–142, https://doi.org/10.1016/j.compositesb.2016.09.094.
[20] M. Del Zoppo, M. Di Ludovico, A. Balsamo, A. Prota, In-plane shear capacity of tuff masonry walls with traditional and innovative Composite Reinforced Mortars (CRM), Construct. Build. Mater. 210 (2019) 289–300, https://doi.org/10.1016/j.conbuildmat.2019.03.133.
[21] F. Ferretti, A. Incerti, A.R. Tilocca, C. Mazzotti, In-plane shear behavior of stone masonry panels strengthened through grout injection and fiber reinforced cementitious matrices, Int. J. Architect. Herit. 15 (2021) 1375–1394, https://doi.org/10.1080/15583058.2019.1675803.
[22] J. Donnini, G. Maracchini, S. Lenci, V. Corinaldesi, E. Quagliarini, TRM reinforced tuff and fired clay brick masonry: experimental and analytical investigation on their in-plane and out-of-plane behavior, Construct. Build. Mater. 272 (2021), 121643, https://doi.org/10.1016/j.conbuildmat.2020.121643.
[23] S. Babaeidarabad, F. De Caso, A. Nanni, URM walls strengthened with fabric-reinforced cementitious matrix composite subjected to diagonal compression, J. Compos. Construct. 18 (2014), 04013045, https://doi.org/10.1061/(asce)cc.1943-5614.0000441.
[24] X. Wang, C.C. Lam, V.P. Iu, Experimental investigation of in-plane shear behaviour of grey clay brick masonry panels strengthened with SRG, Eng. Struct. 162 (2018) 84–96, https://doi.org/10.1016/j.engstruct.2018.02.027.
[25] M. Shabdin, M. Zargaran, N.K.A. Attari, Experimental diagonal tension (shear) test of Un-Reinforced Masonry (URM) walls strengthened with textile reinforced mortar (TRM), Construct. Build. Mater. 164 (2018) 704–715, https://doi.org/10.1016/j.conbuildmat.2017.12.234.
[26] M. Giaretton, D. Dizhur, E. Garbin, J.M. Ingham, F. Porto, In-plane strengthening of clay brick and block masonry walls using textile-reinforced mortar, J. Compos. Construct. 22 (2018) 1–10, https://doi.org/10.1061/(ASCE)CC.1943-5614.0000866.
[27] M. Del Zoppo, M. Di Ludovico, A. Balsamo, A. Prota, Experimental in-plane shear capacity of clay brick masonry panels strengthened with FRCM and FRM composites, J. Compos. Construct. 23 (2019), 04019038, https://doi.org/10.1061/(asce)cc.1943-5614.0000965.
[28] L. Garcia-Ramonda, L. Pelá, P. Roca, G. Camata, In-plane shear behaviour by diagonal compression testing of brick masonry walls strengthened with basalt and steel textile reinforced mortars, Construct. Build. Mater. 240 (2020), 117905, https://doi.org/10.1016/j.conbuildmat.2019.117905.
[29] B. Torres, F.B. Varona, F.J. Baeza, D. Bru, S. Ivorra, Study on retrofitted masonry elements under shear using digital image correlation, Sensors (2020) 20, https://doi.org/10.3390/s20072122.
[30] D. Ungureanu, N. Taranu, D.A. Ghiga, D.N. Isopescu, P. Mihai, R. Cozmanciuc, Diagonal tensile test on masonry panels strengthened with textile-reinforced mortar, Materials 14 (2021) 7021, https://doi.org/10.3390/ma14227021.
[31] F. Ferretti, C. Mazzotti, FRCM/SRG strengthened masonry in diagonal compression: experimental results and analytical approach proposal, Construct. Build. Mater. 283 (2021), 122766, https://doi.org/10.1016/j.conbuildmat.2021.122766.
[32] ASTM E519/E519M-21, Standard Test Method for Diagonal Tension (Shear) in Masonry Assemblages, ASTM International, West Conshohocken, PA, 2021.
[33] R.I.L.E.M. Lum B6, Diagonal Tensile Strength Tests of Small Wall Specimens, 1994.
[34] M. Corradi, A. Borri, G. Castori, R. Sisti, Shear strengthening of wall panels through jacketing with cement mortar reinforced by GFRP grids, Compos. B Eng. 64 (2014) 33–42, https://doi.org/10.1016/j.compositesb.2014.03.022.
[35] P. Meriggi, C. Caggegi, A. Gabor, G. de Felice, Shear-compression tests on stone masonry walls strengthened with basalt textile reinforced mortar (TRM), Construct. Build. Mater. 316 (2022), 125804, https://doi.org/10.1016/j.conbuildmat.2021.125804.
[36] L. Bisby, Fire resistance of textile fiber composites used in Civil engineering, in: Text, Fibre Compos. Civ. Eng., 2016, pp. 169–185, https://doi.org/10.1016/B978-1-78242-446-8.00008-2.
[37] C.C. Papanicolaou, T. Triantafillou, Performance of TRM/TRC systems under elevated temperatures and fire conditions, in: Am. Concr. Institute, ACI Spec. Publ., 2021, pp. 32–46.
[38] F.D.A. Silva, M. Butler, S. Hempel, R.D. Toledo Filho, V. Mechtcherine, Effects of elevated temperatures on the interface properties of carbon textile-reinforced concrete, Cem. Concr. Compos. 48 (2014) 26–34, https://doi.org/10.1016/j.cemconcomp.2014.01.007.
[39] D.A.S. Rambo, F. de Andrade Silva, R.D. Toledo Filho, O. da Fonseca Martins Gomes, Effect of elevated temperatures on the mechanical behavior of basalt textile reinforced refractory concrete, Mater. Des. 65 (2015) 24–33, https://doi.org/10.1016/j.matdes.2014.08.060.
[40] T.H. Nguyen, X.H. Vu, A. Si Larbi, E. Ferrier, Experimental study of the effect of simultaneous mechanical and high-temperature loadings on the behaviour of textile-reinforced concrete (TRC), Construct. Build. Mater. 125 (2016) 253–270, https://doi.org/10.1016/j.conbuildmat.2016.08.026.
[41] N.H. Dinh, S.H. Park, K.K. Choi, Effect of dispersed micro-fibers on tensile behavior of uncoated carbon textile-reinforced cementitious mortar after high-temperature exposure, Cem. Concr. Compos. 118 (2021), 103949, https://doi.org/10.1016/j.cemconcomp.2021.103949.
[42] P. Kapsalis, T. Triantafillou, E. Korda, D. Van Hemelrijck, T. Tysmans, Tensile performance of textile-reinforced concrete after fire exposure: experimental investigation and analytical approach, J. Compos. Construct. 26 (2022) 1–23, https://doi.org/10.1061/(asce)cc.1943-5614.0001162.
[43] J. Donnini, F. De Caso y Basalo, V. Corinaldesi, G. Lancioni, A. Nanni, Fabric-reinforced cementitious matrix behavior at high-temperature: experimental and numerical results, Compos. B Eng. 108 (2017) 108–121, https://doi.org/10.1016/j.compositesb.2016.10.004.
[44] S.M. Raoof, D.A. Bournas, Bond between TRM versus FRP composites and concrete at high temperatures, Compos. B Eng. 127 (2017) 150–165, https://doi.org/10.1016/j.compositesb.2017.05.064.
[45] S.R. Maroudas, C.G. Papanicolaou, Effect of high temperatures on the TRM-to-masonry bond, Key Eng. Mater. 747 KEM (2017) 533–541. https://doi.org/10.4028/www.scientific.net/KEM.747.533.
[46] A. Iorfida, S. Candamano, F. Crea, L. Ombres, S. Verre, P. De Fazio, Bond behaviour of FRCM composites: effects of high temperature, Key Eng. Mater. 817 KEM, 161–166, https://doi.org/10.4028/www.scientific.net/KEM.817.161, 2019.
[47] P.D. Askouni, C.G. Papanicolaou, L. Azdejkovic, Experimental investigation of the trm-to-masonry bond after exposure to elevated temperatures: cementitious and alkali-activated matrices of various densities, Materials 15 (2022), https://doi.org/10.3390/ma15010140.
[48] L. Estevan, F.B. Varona, F.J. Baeza, B. Torres, D. Bru, Textile Reinforced Mortars (TRM) tensile behavior after high temperature exposure, Construct. Build. Mater. 328 (2022), 127116, https://doi.org/10.1016/j.conbuildmat.2022.127116.
[49] M.Y. Koca, G. Ozden, A.B. Yavuz, C. Kincal, T. Onargan, K. Kucuk, Changes in the engineering properties of marble in fire-exposed columns, Int. J. Rock Mech. Min. Sci. 43 (2006) 520–530, https://doi.org/10.1016/j.ijrmms.2005.09.007.
[50] L. Estevan, F.J. Baeza, F.B. Varona, S. Ivorra, Frp confinement of stone samples after real fire exposure, Polymers 12 (2020), https://doi.org/10.3390/polym12102367.

[51] ACI 549.6R-20, Guide to Design and Construction of Externally Bonded Fabric-Reinforced Cementitious Matrix and Steel-Reinforced Grout Systems for Repair and Strengthening of Concrete Structures 549, American Concrete Institute, 2020. ACI Committee.
[52] CNR-DT 215/2018, Guide for the Design and Construction of Externally Bonded Fibre Reinforced Inorganic Matrix Systems for Strengthening Existing Structures, CNR - Advisory Committee on Technical Recommendations for Construction, Rome, Italy, 2020.
[53] UNE-EN 772-1:2011+A1, Methods of Test for Masonry Units - Part 1: Determination of Compressive Strength, 2016, 2016.
[54] UNE-EN 772-6, Methods of Test for Masonry Units - Part 1: Determination of Bending Tensile Strength of Aggregate Concrete Masonry Units, 2002, 2002.
[55] UNE-EN 1015-11:2020, Methods of Test for Mortar for Masonry - Part 11: Determination of Flexural and Compressive Strength of Hardened Mortar, 2020.
[56] Ac434, Acceptance Criteria for Masonry and Concrete Strengthening Using Fiber-Reinforced Cementitious Matrix (FRCM) Composite Systems, ICC Evaluation Service, 2016.
[57] RILEM Technical Committee 232-TDT (Wolfgang Brameshuber), Recommendation of RILEM TC 232-TDT: test methods and design of textile reinforced concrete. Uniaxial tensile test: test method to determine the load bearing behavior of tensile specimens made of textile reinforced concrete, Mater. Struct. 49 (2016) 4923–4927, https://doi.org/10.1617/s11527-016-0839-z.
[58] UNE-EN 1996-1-1:2011+A1:2013, Eurocode 6: Design of Masonry Structures - Part 1-1: General Rules for Reinforced and Unreinforced Masonry Structures, 2013.